# Electrical conductivity of carbon nanotubes grown inside a mesoporous anodic aluminium oxide membrane

*M. Sarno* [a,*], *A. Tamburrano* [b], *L. Arurault* [c], *S. Fontorbes* [c], *R. Pantani* [a], *L. Datas* [c], *P. Ciambelli* [a], *M.S. Sarto* [b]

[a] *University of Salerno and Centre NANO_MATES, Via Ponte don Melillo, 84084 Fisciano (SA), Italy*
[b] *Sapienza University of Rome, DIAEE, CNIS, Via Eudossiana 18, 00184 Rome, Italy*
[c] *Université de Toulouse, CIRIMAT, UPS/INPT/CNRS, LCMIE, 118 route de Narbonne, 31062 Toulouse Cedex 9, France*

A B S T R A C T

Well-aligned, open-ended carbon nanotubes (CNTs), free of catalyst and other carbon products, were synthesized inside the pores of an anodic aluminium oxide (AO) template without using any metallic catalyst. The CNTs and the CNT/AO composites were characterized by scanning and transmission electron microscopy, thermogravimetric analysis, Raman spectroscopy and X-ray diffraction. Particular care was devoted to the reactor design, synthesis conditions, the catalytic role of the templating alumina surface and the preservation of the alumina structure. The transport properties (sorption, diffusion and permeability) to water vapor were evaluated for both the alumina template and the CNT/AO composite membrane. The measured effective electrical volume conductivity of the CNT/AO composite was found ranging from a few up to 10 kS/m, in line with the recent literature. The estimated averaged values of the CNTs-wall conductivity was around 50 kS/m.

## 1. Introduction

The continuous miniaturization of electrical and electronic devices, together with the high integration level and the increase of the working frequencies and power density, is pushing towards innovative solutions for the realization of on chip interconnections and vias in order to avoid in the near future a technological bottleneck [1]. Innovative materials like carbon nanotubes (CNTs) and graphene nanoribbons are being studied as replacements for copper in next-generation high-speed interconnects [2–6].

However, there are several limitations to the practical exploitation of CNT-technology in nanoelectronics, such as the difficulties in controlling the growth process of CNTs having well defined microstructural characteristics and the need of electron beam lithography (EBL) for CNT growth. A possible solution to the aforementioned problems relays in the use of a template-based chemical vapor deposition (CVD) technique [7–9] to fabricate CNT based nano-interconnects components. In this case, the diameter, length and inter-axes distance of the CNTs are controlled by the template morphology, whereas the nanotube wall thickness is dependent directly on the synthesis parameters. The use of metallic catalyst is not needed, and the template growth does not require electron beam lithography (EBL). The resulting process is cost-effective and can be easily implemented at industrial scale. It is also important to notice that the morphological characteristics of the CNT/AO composite membrane combined with the thermal and mechanical properties of the CNTs, enable the use of these materials in application such as heat sinker and strain sensor.

The template-based CVD technique does not require the use of metallic catalyst. Moreover, an additional advantage is that, since the external template surfaces (top, bottom

* *Corresponding author:* Fax: +39 089 964057.
E-mail address: msarno@unisa.it (M. Sarno).

http://dx.doi.org/10.1016/j.carbon.2012.10.063

and edges) are covered by a thin carbon layer all CNTs of the array are electrically connected and bonding with a metal contact become straightforward.

The electrical conductivity of graphitic carbon varies by orders of magnitude, from $10^2$ to $10^5$ S/m, depending on the graphitization degree. A conductivity of $10^4$ S/m has been measured on a single carbon nanotube grown by a templated-based CVD in the channels of alumina membrane (AO) [10].

A significant point related to the growth process regards the proposed catalytic role of the alumina internal structure for the decomposition of hydrocarbons. In a previous work [11] we have indirectly proved that the internal surface of alumina plays a role, by comparing the characteristics of the carbon produced inside and outside the alumina membrane in the same operating conditions. However, the mechanism of CNT formation and the catalytic role of alumina were not definitely proved.

Carbon nanotubes membranes grown on macroporous alumina support have been tested to assess permeability helium, nitrogen and hydrogen [12]. The permeability to water across the membrane is of considerable technological importance for many applications, and at the best of our knowledge it has not been investigated in the literature.

This paper focuses on the synthesis and characterization of AO membranes and of CNT/AO composites obtained by template-based CVD without the use of metallic catalyst. Because alumina during temperature increase is subjected to bending and curling up to break, particular care has been devoted to preserve its flatness, at the macro and consequently micro-scale. This is a prerequisite for a better integration in microelectronic devices. In particular, the thermal expansion coefficient of AO membrane has been investigated and the differences between the top and down alumina surfaces has been discussed. The CNT growing parameters such as temperature, reaction time, total feed flow, hydrocarbon partial pressure, pre-calcination temperature and time, for the first time, as far as we are aware, have been systematically investigated with the objective to preserve the membrane structure. Moreover, specific attention was devoted to the reactor orientation and positioning of the membrane inside the reaction chamber, to favor good fluid dynamic conditions in the reactor [13]. On-line continuous analyzers were used to monitor the reactor outlet composition, in order to get a better knowledge of the mechanism of CNT formation and role of alumina in the growth process.

CNTs and CNT/AO composites were characterized by scanning electron microscopy (SEM) and transmission electron microscopy (TEM), thermogravimetric analysis, Raman spectroscopy and X-ray diffraction (XRD).

Transport properties (sorption, diffusion and permeability) to water vapor were evaluated for both the alumina and the composite membrane for comparison.

Finally, electrical characterization test were performed on the produced CNT/AO composites were tested in order to estimate the conductivity of the carbon nanotubes grown inside the alumina pores. First, the sheet resistance of the graphite layer deposited on both sides of the samples during the nanotube synthesis was measured in order to evaluate its contribution to the total resistance of the specimen. Then, the effective volume conductivity of the composites was measured, and the average conductivity of the sole CNT was calculated.

## 2. Experimental

### 2.1. *Preparation process of the AO membrane*

Two different types of AO porous membranes were prepared. The substrates were always pure aluminium (99.99%), while all chemical compounds used were analytical grade and aqueous solutions were obtained using deionized water.

The first type (F1) was a stand-alone AO membrane with large pores (273 ± 48 nm). The preparation process of the AO templates with large pores was described elsewhere [11,14]. The aluminium substrate (14 mm in diameter and 2 mm thick) was prepared first by sanding, then by annealing under nitrogen atmosphere at 450 °C for 2 h, finally by electropolishing at 25 V for 2 min in a Jacquet mixed solution. Anodization was performed at 185 V for 4 h by an INVENSYS LAMBDA generator (300 V – 5A). The electrolyte was made up of an aqueous phosphoric acid solution (8 wt.%), while a pure aluminium plate was used as cathode. The temperature was regulated at −1.5 °C by a cryostat (HUBER CC2).

After growth of the porous anodic film, the removal of the compact layer was performed using 30 V AC voltage (Universal Power Supply EA-4036) in a phosphoric acid solution and then the substrate was chemically dissolved using a hydrochloric acid solution (18 wt.%) including copper chloride (0.1 mol/L). The membrane was then dipped for 5 min in a phosphoric acid solution and finally rinsed with deionized water.

The second type (F2) was a stand-alone AO membrane with small pores in the range 30–50 nm. The pre-treatment of the substrate and the removal of the compact layer were similar to those performed for the F1 membranes. The main difference was that anodization was performed for 5 h at 28 V in sulphuric acid solution (0.3 M).

### 2.2. *Process of carbon nanotubes growth*

Carbon nanotubes were grown by a template-based ethylene CVD, in the absence of transition metal catalyst, in a laboratory apparatus equipped with: (i) mass flow controllers to feed constant gases flow rates in order to have a better process control, (ii) an electrically heated and temperature controlled flow microreactor, fed by ethylene-nitrogen gas mixture (see Figs. 1 and 2 for details), arranged vertically to better control the fluid dynamics of the reactor forcing the flow to pass through the membrane, (iii) on-line continuous specific analyzers for reactor outlet gas products (ABB analysers that permit to measure $C_2H_4$, $C_2H_2$, $CH_4$ and $H_2$ concentrations in the effluent stream on line during the reaction). A vertical arrangement that does not suffer from longitudinal diffusive limitations along the reactor axes was chosen, permitting the control of the thickness and concentration homogeneity of the boundary layer (the stagnant layer established in the steady state conditions at the membrane interface). One membrane (of both types F1 and F2) was placed on a sintered support in an isothermal zone of the reactor. Starting from the results of our previous work [15] (in which we conclude

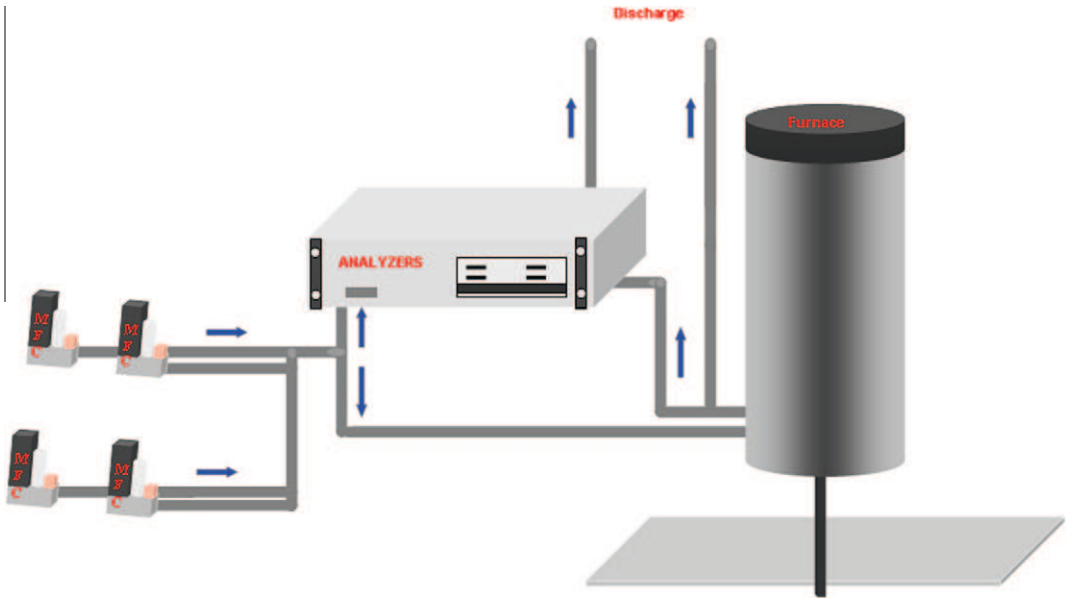


**Fig. 1 – Scheme of the experimental apparatus for carbon nanostructures growth.**

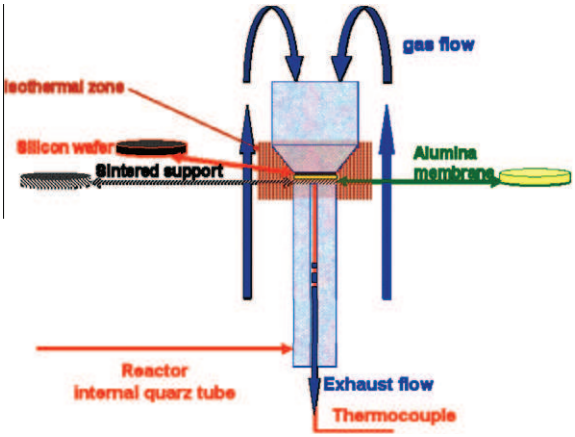


**Fig. 2 – Details of the microreactor for carbon nanostructures growth.**

that carbon order increases by increasing hydrogen concentration and from using different hydrocarbons along the scale acetylene, propylene, ethylene and methane), and synthesis temperatures, we chosed to fed ethylene in $N_2$, as a good compromise between carbon quality and cost. Ethylene, more reactive than methane, was fed in N2 and not in the more expensive $H_2$, also to favor its conversion at temperature of about 800 °C. For Test 20 (see Table 1) commercial membranes (Anodisc; sample diameter:13 mm; pore diameter: 0.2 mm) manufactured by Whatmann (WAOs) were used. In our previous paper [11] we demonstrated that the TG–DTG profiles of CNT/AO composites materials obtained by using commercial and prepared membranes are practically superimposed.

Due to the necessity of maintaining the membrane flatness after synthesis, the effect of the operating conditions (synthesis time, temperature, ethylene partial pressure in $N_2$ and pretreatment time) was investigated (see Table 1). In particular, for all the tests the total feed flow was 200 Ncc/min, the ethylene partial pressure ranged from 10 to 30 v/v.%, the temperature form 750 to 950 °C.

Carbon nanotubes formed during the synthesis were obtained by treating the CNT/AO composite with 20 ml of 50 wt.% HF aqueous solution for 24 h in order to dissolve the alumina template and the solid residue was washed in distilled water, centrifuged and finally dried at 353 K for 12 h.

### 2.3. *Physico-chemical characterization of composite and recovered carbon*

The produced CNT/AO composites and carbon nanotubes recovered were characterized using various techniques. Scanning Electron Microscopy (SEM) pictures were obtained with a LEO 1525, while Field Emission Gun Scanning Electron Microscope views were performed by using FEG-SEM JEOL JSM 6700F.

Transmission electron microscopy (TEM) images were obtained with a Jeol 1200 EX2 microscope. The preparation of samples for TEM observation involved sonication in ∼1 ml of ethanol for 2–5 min and deposition on a carbon grid. The accelerating voltage of the electron beam was 200 kV.

Simultaneous TG–DTG analysis was performed with a Thermogravimetric Analyser SDTQ 500 TA Instruments. The measurements were performed in the range 25–900 °C, with 10 °C/min heating rate under flowing air. Raman spectra were obtained at room temperature with a microRaman spectrometer Renishaw in Via (514 nm excitation wavelength). X-ray diffraction measurements (XRD) were performed with a Brucker D8 X-ray diffractometer (equipped with a continuous scan attachment and a proportional counter) with Ni-filtered Cu Ka radiation ($\lambda$ = 1.5405 Å).

### 2.4. *Transport properties of AO membrane and composite*

Transport properties to water vapor (sorption, diffusion and permeability) were evaluated using a microbalance SMS DVS

**Table 1 – Operating conditions for CNTs growth.**

| Tests | Sample name | Calcination temperature (°C) | Calcination time (min) | Membrane family | Reaction temperature (°C) | Reaction time (min) | Total feed flow (Ncc/min) | $C_2H_4$ (vol.%) |
|---|---|---|---|---|---|---|---|---|
| 1 | M1 | – | – | F1 | 950 | 30 | 200 | 10 |
| 2 | M2 | – | – | F1 | 900 | 30 | 200 | 10 |
| 3 | M3 | | | F1 | 900 | 5 | 200 | 10 |
| 4 | M4 | – | – | F1 | 870 | 30 | 200 | 10 |
| 5 | M5 | | | F1 | 870 | 5 | 200 | 10 |
| 6 | M6 | – | – | F1 | 835 | 30 | 200 | 10 |
| 7 | M7 | | | F1 | 835 | 5 | 200 | 10 |
| 8 | M8 | – | – | F1 | 800 | 30 | 200 | 10 |
| 9 | M9 | – | – | F1 | 800 | 60 | 200 | 20 |
| 10 | M10 | – | – | F1 | 750 | 60 | 200 | 30 |
| 11 | M11 | – | – | F1 | 750 | 270 | 200 | 30 |
| 12 | M12 | 835 | 30 | F1 | – | – | – | – |
| 13 | M13 | 835 | 20 | F1 | 825 | 10 | 200 | 10 |
| 14 | M14 | 835 | 10 | F1 | 825 | 10 | 200 | 10 |
| 15 | M15 | 835 | 10 | F1 | 825 | 10 | 200 | 20 |
| 16 | M16 | | | F1 | 825 | 10 | 200 | 20 |
| 17 | M17 | | | F1 | 825 | 10 | 200 | 30 |
| 18 | M18 | – | – | F1 | 810–820 | 10 | 200 | 30 |
| 19 | M19 | – | – | F2 | 810–820 | 10 | 200 | 30 |
| 20 | M20 | – | – | WAO | 850 | 10 | 200 | 30 |
| 21 | M21 | – | – | WAO | 850 | 40 | 200 | 30 |

Advantage-2 system. This system has a sensitivity of ±1.0 μg, and allows the measurement of mass changes due to sorption or desorption of vapor molecules. The tests were conducted using water vapor in a nitrogen atmosphere at 30 °C on previously dried samples. The experimental protocol considered steps of relative humidity in the following sequence: 30% (corresponding to a partial pressure of water of 0.013 bar), 60% (corresponding to a partial pressure of water of 0.026 bar), 30%, 0% (pure dry nitrogen). Each step lasted until mass stabilization.

### 2.5. *Electrical conductivity measurements*

Two different set-ups were used to characterize the electrical properties of the CNT/AO composites and to extract the dc electrical conductivity of the CNTs grown inside the membrane pores.

The first test set-up implements the four-point probe method (ASTM F390–398) to measure the sheet electrical resistance of the carbon layer deposited over the surface of alumina membranes at room temperature. The probe head used for the test is composed by four collinear equally spaced tungsten carbide tips, and it is secured to the Signatone S301 stand arm. The system is connected to a Keithley 6221 dc/ac current source and a Keithley 2182a nanovoltmeter. The two instruments were remotely controlled by a PC station, and the measurement was performed in delta-mode to compensate for thermoelectric voltages. The nanovoltmeter was triggered to record the voltage drop between the two inner tips of the probe as the dc current was sourced through the two outer tips with alternating polarity. The absolute values of the readings were then averaged and used to calculate the average sample resistance. The sheet resistance was calculated multiplying the average sample resistance by a proper correction factor, which depends on the specimen and probe geometries. Finally, the bulk conductivity of the film was obtained as the inverse of the product between its sheet resistance and thickness.

The dc volume conductivity of the CNT/AO composite specimens was measured by applying the direct voltmeter-ammeter method. The test fixture was realized by contacting the top and bottom faces of the circular-shaped samples, having diameter of 10 mm. At first, the bottom face of each specimen was completely covered with highly conducting silver paint characterized by volume conductivity of nearly 9 kS/cm. The samples were then baked at 70 °C in oven for 10 min, glued on a Cu electrode using a conducting epoxy with volume resistivity of about 2 mΩ cm, and finally exposed to an additional thermal cycle. Adopting a ring-shaped mask, the top electrode was attached with conducting epoxy on a circular area of 5 mm in diameter, precisely in the center of the specimen top surface. Four-wire resistance measurements were finally performed connecting the electrodes to a Keithley AC–DC current source and a Keithley nanovoltmeter as sketched in Fig. 3a. The equivalent electrical circuit of the test set up is reported in Fig. 3b, in which: $R_{top}$ and $R_{bottom}$ are the total contact resistance of the top and bottom face of the membrane, accounting for the external carbon layer, the silver paint and the silver paste; $R_{border}$ is the equivalent resistance of the carbon film surrounding the lateral side of the membrane; $R_{CNT\_tot}$ is the total dc resistance of all CNTs grown inside the membrane pores and parallel connected. The effective electrical conductivity $\alpha_{CNT}$ of the CNTs is obtained by the following expression:

$$\sigma_{CNT} = \frac{h_m}{\delta_p A_m \pi [d_{CNT}(2r)_p - d_{CNT}] R_{CNT_{tot}}} \quad (1)$$

where $d_{CNT}$ is the average wall thickness of the CNTs, $r_p$ is the pore radius, $\delta_p$ is the pore density, $A_m$ and $h_m$ are the surface area and thickness of membrane, respectively.

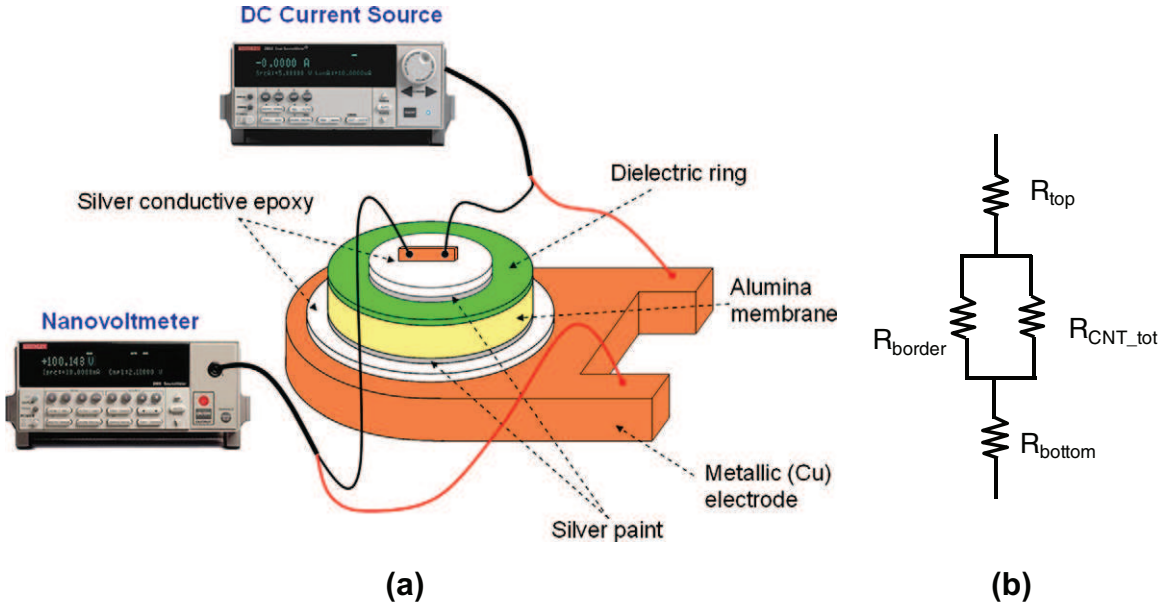


**Fig. 3 – (a) Sketch of the electrode system for the effective volume conductivity measurements of composites (not to scale). (b) Equivalent electrical circuit.**

## 3. Results and discussion

### 3.1. *Control of the flatness of CNT/AO membrane*

During temperature increase from 25 to 950 °C, i.e. the maximum value used for the subsequent CNTs growth, the membrane undergoes deformation: bending (Fig. 4a), followed by curling (Fig. 4b) up to break (Fig. 4c). This bending phenomenon was previously noted by Fernandez-Romero [16] and by ourselves [11]. It is likely caused by the conversion from amorphous to polycrystalline material [16] and the successive change of the cell parameters of the alumina crystal structure, as well as by the change of the thermal expansion coefficient. In particular, an XRD study was effected, in the 700–1000 °C temperature range, of the well-isolated peak at 42.7 $2\theta$ (at 900 °C) in order to obtain the coefficient of thermal expansion ($\alpha$) of the F1 membrane. From the peak maximum shift as a function of the temperature, the coefficient of the membrane was estimated as $16 \times 10^{-6}\,K^{-1}$. This value is in disagreement with the usual one ($5.10^{-6}\,K^{-1}$ [17]) but in accor-

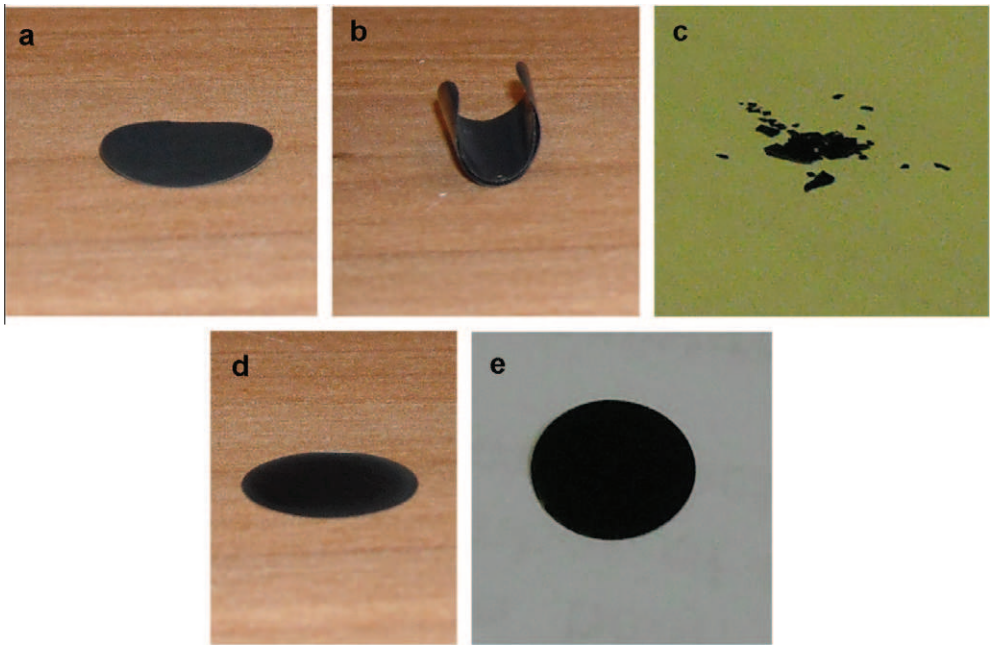


**Fig. 4 – Photos of: test 7 (a), test 5 (b), test 3 (c), flat CNTs/Family2 membrane (M18) (d) and flat CNTs/Family3 membrane (M19) (e).**

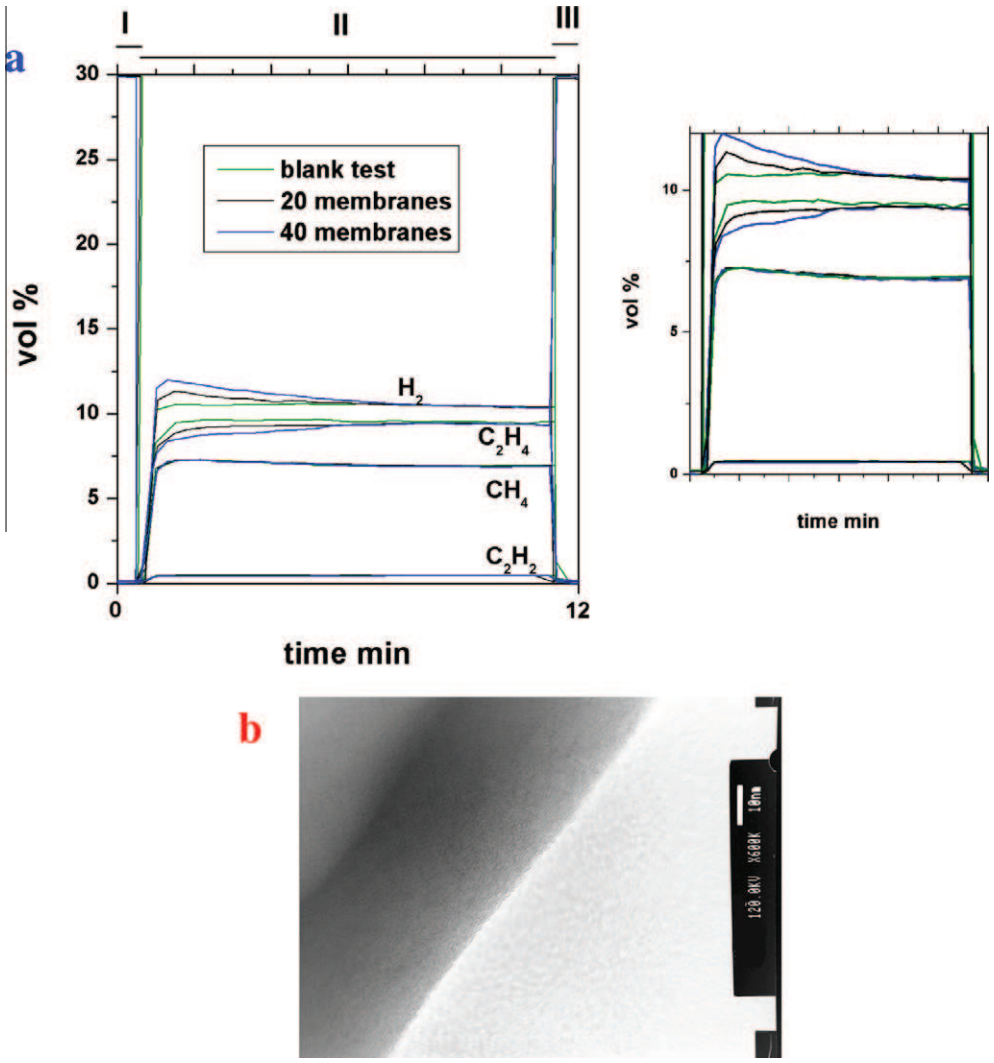


**Fig. 5 – Blank test in comparison with the two tests performed in presence of 20 and 40 membranes (10 min at 825 °C, 200 Ncc/min of ethylene 30 v/v.% in $N_2$). (a)TEM image of ananotube from test 21 (b)**

dance with values obtained for unsupported anodic films, showing tortuous porosity, obtained with sulphuric acid solutions: $14.136 \times 10^{-6}\ K^{-1}$ [18] and $13 \times 10^{-6}\ K^{-1}$ [19].

If the membrane is considered as homogeneous, the bending effect cannot be explained neither by the sole coefficient of thermal expansion, nor only by the crystallization phenomena, nor by successive parameter changes within the alumina crystal structure. This phenomenon can also result from the morphology difference between the two faces of the AAO membrane [11].

In any case, considering the necessity to keep the membrane flatness after the CNT synthesis, different operating conditions were investigated (Table 1). We found that only few minutes at 900 °C were sufficient to produce fragmentation of the membrane (test 3). At 870 °C membrane curling was observed (test 5) and at 835 °C bending was evidenced (test 7). It is also resulted that at 800 °C no CNTs formed, neither at longer synthesis time, neither increasing the partial pressure of hydrocarbon in the feed (test 8 and 9).

Trying to preserve the membrane flatness and to deposit CNTs in its channels, we explored the effect of a calcination process before the synthesis with the membrane pressed between two Si wafers, and at temperature of 10 °C higher than that of the synthesis. For this purpose four membranes were, one by one, gently pressed between two silicon wafers (the sandwich wafer/membrane/wafer was held together by a clamp) and treated at various temperatures in a furnace. These tests showed that a temperature of 835 °C (test 12) and an exposure time of 10 min were the minimum conditions to activate the phenomena described above.

To obtain a better control of the calcination step and to simplify the process, in test 13 the membrane was positioned between two silicon wafers and on the sintered support in the reactor, and then the CNTs synthesis was performed at 825 °C. Further experiments were carried out reducing the calcination time to 10 min (tests 14 and 15), or using the support itself to form the membrane (tests 16 and 17). We found that the results of tests 15 and 16 were very similar, and that a

slight bending of the membrane was still present in test 16. Final optimized conditions for CNT growth in flat membrane (Fig. 4d) were achieved by pressing the membrane between a Si wafer and the rector sintered support (on the silicon wafer was put a load of 50 g) and performing the CVD in the temperature range 810–820 °C for 10 min under 200 Ncc/min, ethylene concentration v/v.% = 30% (test 18). Faster pre-treatment (15 min to reach 810 °C instead of 20 min for F1 membranes) allowed to obtain CNTs in type F2 flat membranes (test 19 Table 1), as shown in Fig. 4e. The composites materials from tests 18 and 19 are labeled in the following M18 and M19, respectively.

### 3.2. *Study of the catalytic role of the alumina channels surface*

Since in the non-catalytic CVD process the carbon precursors are deposited on the pore walls by hydrocarbon decomposition, a catalytic role of the template membrane has been supposed [20].

The approach was based on the careful analysis of the trend of $C_2H_4$ and $H_2$ composition, as monitored by the continuous gas analyzers and of the concentration of $C_2H_2$ and $CH_4$, two of the hydrocarbon fractions most likely formed by ethylene decomposition [21,22]. A typical profile of $C_2H_4$, $C_2H_2$, $CH_4$ and $H_2$ concentration during a blank test (in empty reactor) in the same conditions of test 20 (see paragraph 2.2) is shown in Fig. 5.

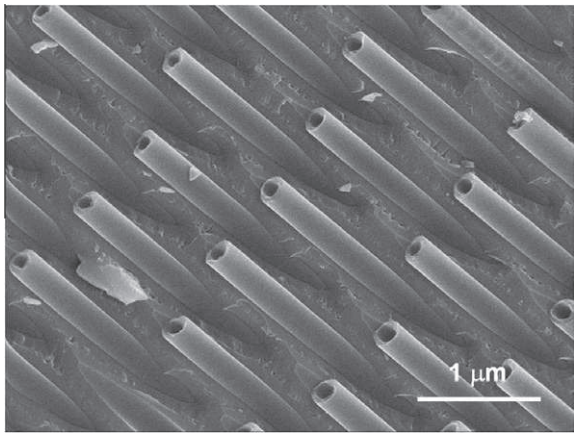


**Fig. 7 – FEG-SEM cross sectional view of CNT/AO (sample M18).**

We can distinguish three time-distinct phases:

- Pre-reaction phase (I): the reaction gas is fed to the analyzers. All concentration profiles are close to zero, except for the initial ethylene concentration (30 v/v.%).
- Reaction phase (II): the gas flows through the reactor. After reaching a steady state conditions, the ethylene concentration stabilizes at 9 vol.%. The reduction of ethylene concentration is due to the thermal decomposition in the

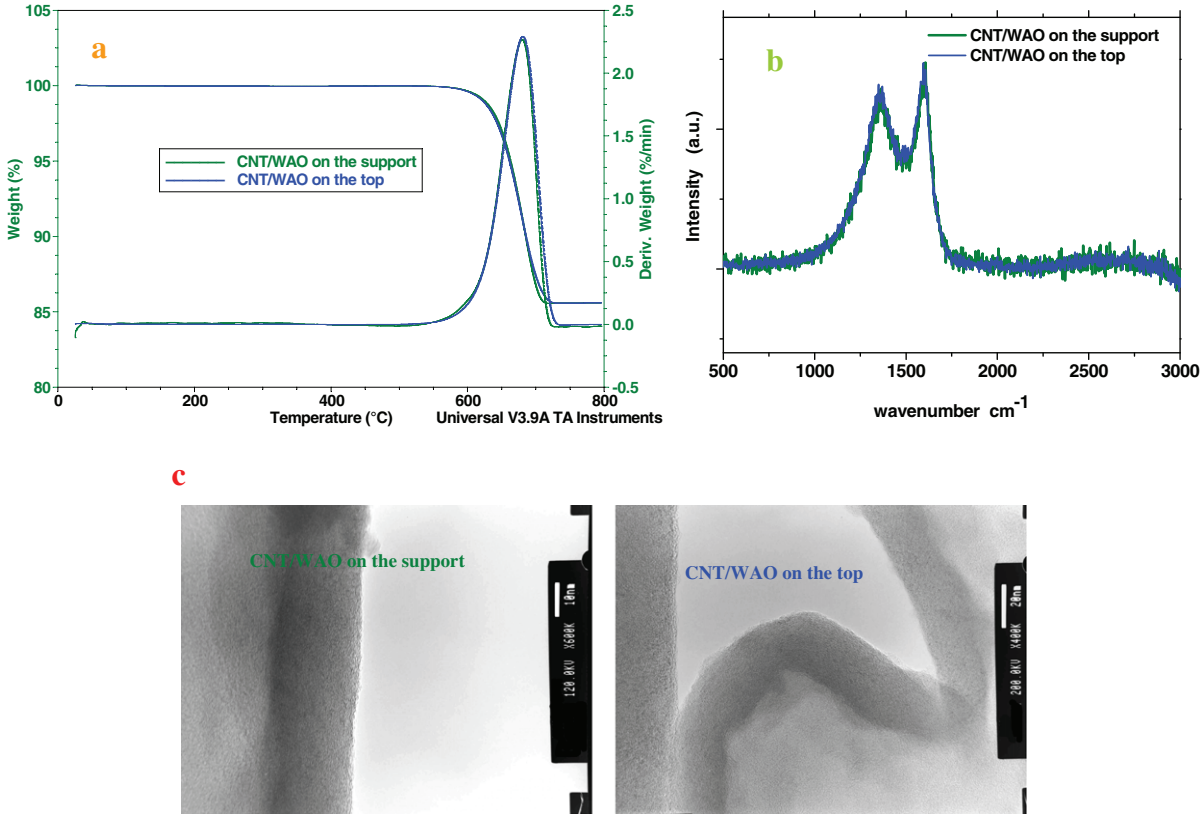


**Fig. 6 – TG–DTG profiles (a), Raman spectra (b) and TEM images (c) of two different membranes, from the test with 40 membranes in the same operating conditions of test 20.**

homogeneous phase, leading, in part, to the formation of hydrogen and carbon. We can observe also the presence of methane and acetylene in the reactor outlet gas.

- Post-reaction phase (III): the run is stopped and the gas stream is sent directly to the analyzers (not through the reactor) to verify that the gas concentrations return to the values of the pre-reaction phase.

In Fig. 5, the concentrations profiles of the four gases during two tests performed in the presence of 20 or 40 membranes, stacked one on top, to highlight the effects detected by the analyzers, in the same operating conditions of test 20, are also reported. It is observed that the profiles of ethylene and hydrogen in the presence of membranes do not coincide with those of the blank test, during the first minutes of the synthesis. The ethylene and hydrogen profiles reached the blank test plateau after ~7 min of synthesis, and before were shifted (i) to lower values, in the case of ethylene (indicating an increased conversion), (ii) to higher values, in the case of hydrogen. The shift was more and more evident as higher was the number of membranes. On the contrary, the methane and acetylene concentration profiles resulted unaltered, and in general overlapped those of the blank test.

Thus, the presence of the membranes determines an increase of the ethylene conversion to C and $H_2$, as indicated by the $H_2$ profiles and the overlapping of the $CH_4$ and $C_2H_2$ signals. This behavior lasted only the first few minutes, likely due to the progressive covering of the alumina active sites. On the contrary, the slower homogeneous thermal ethylene decomposition continued contributing to the progressive thickening of the tube walls [23].

Moreover, in Figs. 5b and 6c TEM the images of the CNTs from the test 21 and of the CNTs from test 20 are shown, the thickness of the tubes from test 20 is about 25 nm and about 38 for the CNTs form test 21, much more smaller than the 100 nm expected after 40 min of synthesis, suggesting that alumina has a catalytic effect. The most probably explanation was that when alumina surface results completely covered of carbon a different mechanism no-alumina affected regulates the formation of the residual walls.

### 3.3. *Reactor design and mass transport conditions effect*

To obtain the uniformity of the deposited carbon on the alumina surface (thickness, quantity…) it is necessary to control as much as possible the diffusion phenomena. It is essential to avoid that geometrical effects and the geometry itself of the CVD chamber play a critical role during the overall synthesis. Therefore we opted for a vertical reactor arrangement, to control the uniformity of the mass transport conditions on the membrane surface and choosing a feed rate that ensured to work as much as possible near a chemical regime. An evidence supporting the absence of a concentration gradient in our reactor is the observation that the amount and quality of deposited carbon is the same for different reactor heights. In particular, Fig. 6 shows the results of the TG–DTG analysis, the Raman Spectra and TEM images of two different membranes from the test with 40 membranes in the same operating conditions of the test 20, stacked in the reactor. The TG–DTG curves are similar and generally overlap, indicating that the carbon nanotube masses and quality are uniform, exhibiting a single step of weight loss due to the combustion of the carbon material. The two Raman spectra are practically superimposable, confirming the results of the thermogravimetrical analysis, while the high resolution transmission electron microscopy images show nanotubes walls with the same thickness and structural characteristics (see below for a detailed discussion about the results coming from Raman and TEM characterizations).

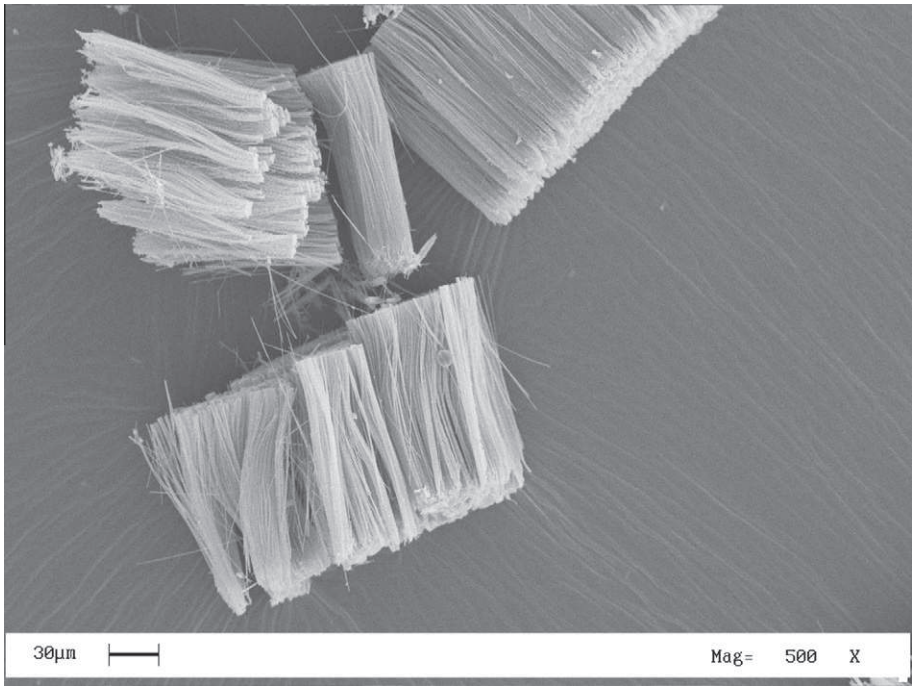


**Fig. 8 – CNTs after HF alumina removal (sample M18).**

### 3.4. *Physico-chemical characterization of composite and recovered carbon*

A complete characterization of the CNT and the composites material was performed. The FEG-SEM cross sectional view of the CNT/AO composite shows a highly ordered composite (Fig. 7), each pore contains a single CNT with diameter closely tuned by the pore walls.

In Fig. 8 CNTs of M18, obtained after the alumina removal by HF solution, are shown. The TEM image of Fig. 9a and b give evidence of the nanotube morphology of the produced carbon, showing the hollow core of the tubes. In particular, it is visible the uniformity of produced nanotubes in terms of diameters and thickness along the tube axis. The structure of the CNT walls is zoomed in Fig. 9(c), which shows twisted walls in the direction of the nanotube axis [11].

The TG profile of M18 (Fig. 10) shows in the range 25–800 °C a single step of weight loss due to the combustion of the carbon material, indicating the presence of a substantially single carbon phase in the sample. Residual mass over 800 °C represents the inorganic fraction (membrane residue).

The Raman spectrum of M18 shown in Fig. 11 (the spectrum of M19 not shown here practically overlaps with that of M18), collected with a 514 nm laser wavelength, exhibits the typical Raman profile of CNT (D and G not separated and partially overlapped). The D band is indicative of defect in the nanotube walls (i.e. carbonaceous impurities with $sp^3$ bonding, broken $sp^2$ bonds in the sidewalls) [24,25]. The $I_D/I_G$ intensity ratio, that is a measure of disorder amount, equal to 0.79, results comparable with literature data [20,27]. The fact that the two peaks have nearly identical magnitude indicates the presence of nanocrystalline graphite with domain size less than 10 nm [11].

The XRD pattern in Fig. 12 shows the non crystalline nature of the membrane in M18 after the CNTs synthesis, partially justifying the absence of macroscopic membrane deformation. The most intense carbon materials peaks at about 25° and 43° are also visible.

### 3.5. *Transport properties (sorption, diffusion and permeability)*

The recording of mass evolution with time during the steps of relative humidity is reported in Fig. 13 for an F2 membrane and M19. It can be noticed that the composite materials required a much longer time to reach a mass stabilization. The carbon–water interaction in the absence of functional group, such as –COOH [26], is due to van der Waals-like force [27]. Sample M19 presents a typical sorption curve, with a gradual increase (during sorption) and decrease (during desorption) of the mass.

F2 presents a peculiar sorption curve: during the first humidity step (namely at zero time), a sudden increase of mass is recorded, followed by a less steep increase at longer times. Similarly, when the sample is dried again (namely at the beginning of the last step), this sudden increase is nearly immediately recovered. This phenomenon deserves further investigations, but it can be interpreted with a sudden occupation of a portion of free volume by water molecules. This occupation is then followed by a typical sorption of water inside the sample. When the sample is dried again, the mentioned portion of free volume is nearly suddenly emptied.

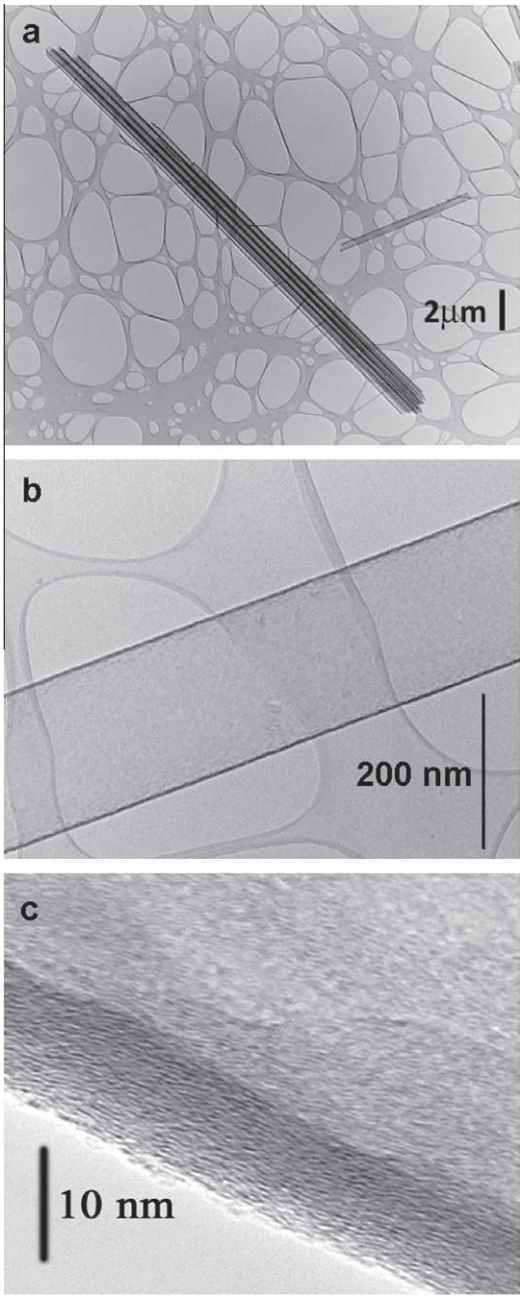


**Fig. 9 – TEM-HRTEM images of carbon nanotubes (sample M18).**

The quantity of water present inside the samples at the end of each relative humidity step (Mw), namely the equilibrium water content, was calculated from the data reported in Fig. 13 and are reported in Fig. 14 with respect to the mass of dry sample. It can be noticed that the quantity of water absorbed by F2 is slightly larger with respect to the other sample, even if the quantities are surely comparable. Both samples present a slight hysteresis.

The sorption coefficient S, calculated from the slopes of the plots reported in Fig. 14 for both samples, was 20.8 g/(100 g of dry sample)/bar for M19 and 22.9 g/(100 g of dry sam-

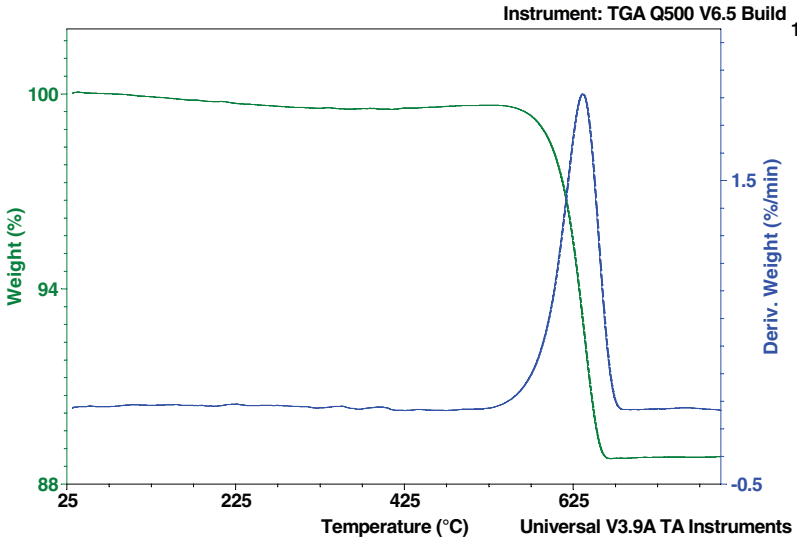


**Fig. 10 – TG–DTG analysis of M18.**

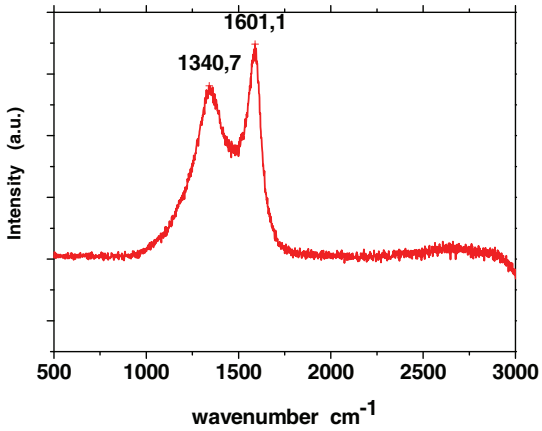


**Fig. 11 – Raman Spectrum of M18 collected with 514 nm laser wavelength.**

ple)/bar for F2. By assuming the density of dry samples to be 4 g/cm$^3$ for alumina membrane and 3.6 g/cm$^3$ for M19 (the mean weight density of the composite, considering for CNTs a density of 2 g/cm$^3$), the sorption coefficient was 736 cm$^3$ (STP)/(cm$^3$ bar) for M19 and 1140 cm$^3$(STP)/(cm$^3$ bar) for the starting membrane.

The diffusivity $D$ was calculated by analyzing the mass changes at each step of relative humidity. The equation used to evaluate the diffusivity was:

$$\ln\left[\frac{d}{dt}\left(\frac{M(t)-M_0}{M_\infty-M_0}\right)\right]=\ln\left(\frac{8D}{h^2}\right)-\frac{\pi^2 D}{h^2}t$$

in which $M(t)$ is the mass of the sample at each time, $M_0$ is the value at the beginning of the humidity step, $M_\infty$ is the value of the mass at stabilization (equilibrium), h is the thickness of the sample. The previous equation is valid for times such that the ratio $\left(\frac{M(t)-M_0}{M_\infty-M_0}\right)$ is larger than about 0.4.

Plotting $\ln(d\,Mt/dt)$ vs time, the value of $D$ (cm$^2$/s) is calculated at each partial pressure from the slope of the curve.

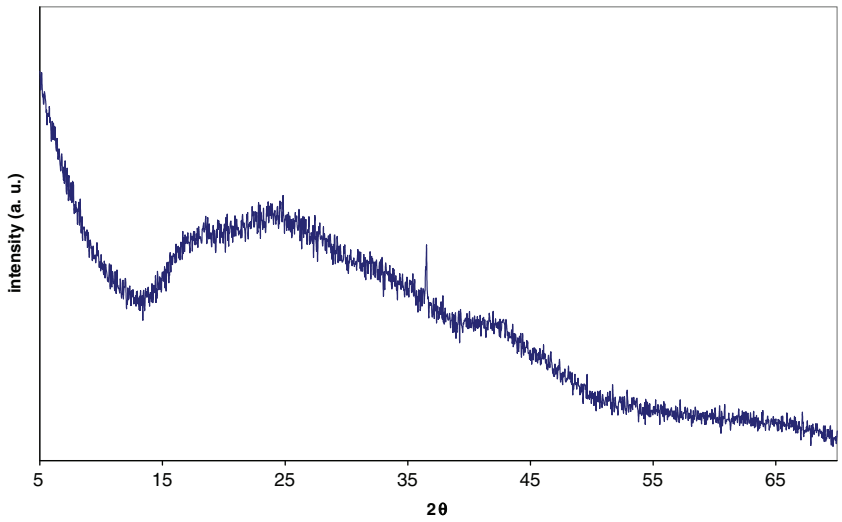


**Fig. 12 – X-ray diffraction pattern of M18.**

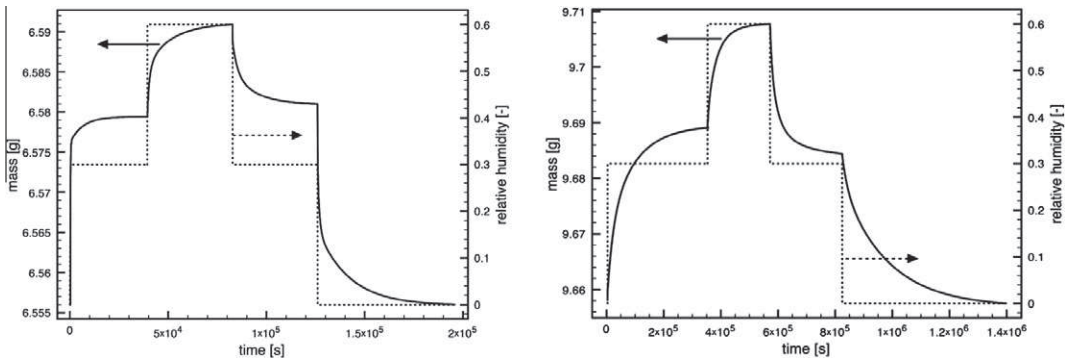


**Fig. 13 – Mass evolution with time during the steps of relative humidity.**

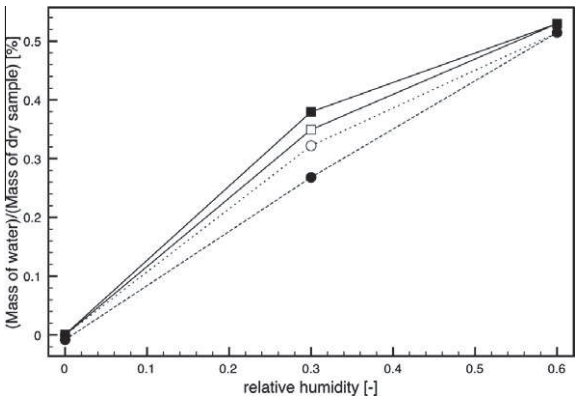


**Fig. 14 – Sorption isotherm for both samples. Squares: F2; Circles: M19. Empty symbols: sorption. Filled Symbols: desorption.**

The results, summarized in Fig. 15, show that M19 gives a diffusivity larger by about a factor 5 than F2. The average values of diffusivity were: $6.8 \times 10^{-10}$ cm$^2$/s for M19 and $1.6 \times 10^{-10}$ cm$^2$/s for F2. The composite CNT/AO shows an almost significant improvement of the water transport properties, although the internal diameter of the CNTs is about 30 nm, larger in comparison to the size of the water molecules. To achieve enhanced transport properties reported by previous studies [28] related to the unique low-friction properties and hydrophobic properties of CNT surface it is crucial to decrease the size of CNT internal diameter to the size of transported molecules [29].

Permeability values to water vapor were evaluated as product of sorption and diffusion:

$$P = SD$$

The results obtained are $5 \times 10^{-7}$ cm$^3$(STP)/(cm s bar) for M19, and $1.82 \times 10^{-7}$ cm$^3$(STP)/(cm s bar) for F2. M19 is fairly more permeable to water vapor, likely due to an enhanced hydrophobicity of the sample due to carbon.

### 3.6. *Electrical tests*

#### 3.6.1. *Surface conductivity of the external carbon layer*

The dc resistance of the external carbon layer of CNT/AO composite samples obtained in the tests 18 and 19 was measured. The I–V characteristic of the tested samples is reported in Fig. 16. The dc conductivity of the carbon film deposited over the surface of samples M18 and M19 was evaluated assuming an average thickness of the external carbon layer varying between 15 and 40 nm, as deduced from SEM and TEM analysis. The obtained results show values in the range of 40–50 kS/m.

#### 3.6.2. *DC conductivity of the CNTs grown inside the membrane pores*

The dc volume conductivity of samples M18 and M19 was measured using the set-up described in Section 2. Fig. 17 shows that the silver conducting paint is composed by silver

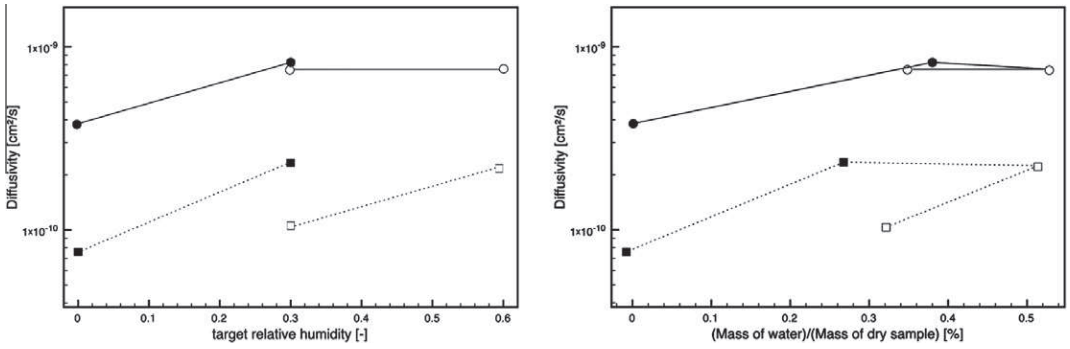


**Fig. 15 – Diffusivity. Squares: F2; Circles: M19. Empty symbols: sorption. Filled Symbols: desorption. Left: data versus relative humidity. Right: data versus equilibrium water content.**

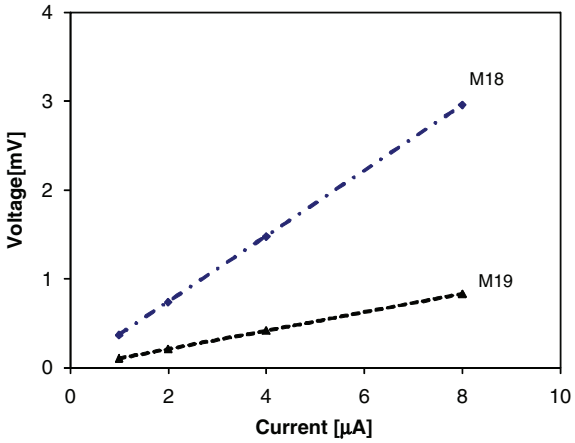


**Fig. 16 – I–V characteristic of samples M18 and M19.**

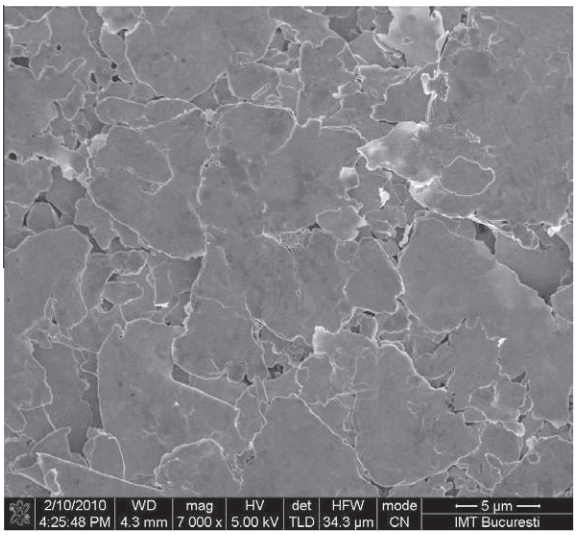


**Fig. 17 – SEM image of the silver paint deposited over the surface of sample M18.**

particles having diameter in the range of several microns, and it confirms that once deposited on the surface of the porous substrate silver cannot pass through the holes of the membrane.

Considering that the silver paint has a conductivity of 900 kS/m and the silver paste of 238 kS/m, it results that the electrical volume conductivities of the CNTs grown in membranes M18 and M19 is about 52 and 58 kS/m, in the hypothesis that according to TEM analysis the average CNT wall thickness is of 10 and 7 nm respectively for the two different samples.

## 4. Conclusion

CNTs (one nanotube for each channel) were synthesized by CVD in the channels of well ordered alumina membranes. The length of the CNTs is coincident with the membrane thickness, their external diameter is close to the diameter of the membrane holes, and the CNT wall thickness adjustable by changing the reactor operating conditions.

The dissolution of the membrane gives bundles of parallel tubes, opened and aligned without macroscopic defects. The external diameter of the tubes is uniform and there is no evidence of amorphous carbon. The nanotubes reflect the internal structure of the membrane channels.

Bending of the CNT/AO sample was observed at the high temperature used for the CNTs growth. The respective influences of the thermal expansion coefficient ($16 \times 10^{-6}\,K^{-1}$), the conversion from amorphous to polycrystalline alumina allotropic phases, the morphology difference between both faces of the AO membranes are still in discussion. In any case, a "forming process", with the membrane between a silicon wafer and the sintered reactor support, during the synthesis performed in a temperature range 810–820 °C, successfully avoid curling of the membranes during heating. Flat membranes were obtained after synthesis. The nanotube shape of the produced carbon is demonstrated by TEM characterization; twisted walls in the direction of the nanotube axis are visible as well.

The on-line analysis of the reactor outlet gas has given useful information to better understand the mechanism of CNTs formation.

The measurement of transport properties to water vapor showed that diffusivity is much higher for the carbon containing sample, likely due to enhanced hydrophobicity. In any case, both samples present a measurable permeability to water vapor.

We found values of the effective electrical volume conductivity of the composite ranging from a few up to ten kS/m, comparable with the recent literature. The averaged conductivity of the CNTs was also calculated showing values around 50 kS/m.

## Acknowledgments

This work has been performed within the European research project CATHERINE – Carbon nAnotube Technology for High-speed nExt-geneRation nano-InterconNEcts – under grant agreement no. 216215. The authors are grateful to Dr. Adrian Dinescu for providing HR SEM images of the surface of the silver pain deposited over the membrane.

## REFERENCES

[1] Naeemi A, Sarvari R, Meindl JD. Performance comparison between carbon nanotube and copper interconnects for gigascale integration (GSI). IEEE Electron Device Lett 2005;26(2):84–6.
[2] Massoud Y, Nieuwoud A. Modeling and design challenges and solutions for carbon nanotube-based interconnect in future high-performance integrated circuits. ACM J Emerg Technol Comput Syst 2006;2(3):155–96.
[3] D'Amore M, Sarto MS, Tamburrano A. Fast transient analysis of next-generation interconnects based on carbon nanotubes. IEEE Trans EMC 2010;52(2):496–503.
[4] Atthipalli G, Tang Y, Star A, Gray JL. Electrochemical characterization of carbon nanotube forests grown on copper foil using transition metal catalysts. Thin Solid Films 2012;520(5):1651–5.

[5] Fan S, Chapline MG, Franklin NR, Trombler TW, Cassell AM, Dai H. Self-oriented regular arrays of carbon nanotubes and their field emission properties. Science 1999;283(5401):512–4.
[6] Atthipalli G, Epur R, Kumt PN, Yang M, Lee JK, Gray JL. Nickel catalyst-assisted vertical growth of dense carbon nanotube forests on bulk copper. J Phys Chem C 2011;115(9):3534–8.
[7] Che G, Lakshmi BB, Martin CR, Fisher ER. Chemical vapor deposition based synthesis of carbon nanotubes and nanofibers using a template method. Chem Mater 1998;10(1):260–7.
[8] Ciambelli P, Sannino D, Sarno MB, Nagy J. Characterisation of nanocarbons produced by CVD of ethylene in alumina or alumino-silicate matrices. Adv Eng Mater 2004;6(10):804–11.
[9] Ciambelli P, Sannino D, Sarno M, Fonseca A, Nagy JB. Hydrocarbon decomposition in alumina membrane: an effective way to produce carbon nanotubes bundles. J Nanosci Nanotechnol 2004;4(7):779–87.
[10] Mattia D, Rossi MP, Kim BM, Korneva G, Bau HH, Gogotsi Y. Effect of Graphitization on the wettability and electrical conductivity of CVD-carbon nanotubes and films. J Phys Chem B 2006;110(20):9850–5.
[11] Ciambelli P, Arurault L, Sarno M, Fontorbes S, Leone C, Datas L, et al. Carbon nanotubes quality enhancement by controlling preparation conditions of ordered mesoporous AAO membranes and optimizing CVD operational parameters. Nanotechnology 2011;22(26):265613/1–265613/12.
[12] Mia W, Lina YS, Li Y. Vertically aligned carbon nanotube membranes on macroporous alumina supports. J Membr Sci 2007;304(1–2):1–7.
[13] Sarno M, Sannino D, Leone C, Ciambelli P. Evaluating the effects of operating conditions on the quantity, quality and catalyzed growth mechanisms of CNTs. J Mol Catal A: Chem 2012;357:26–38.
[14] Le Coz F, Arurault L, Fontorbes S, Vilar V, Datas L, Winterton P. Chemical composition and structural changes of porous templates obtained by anodizing aluminium in phosphoric acid electrolyte. Surf Interface Anal 2010;42(4):227–33.
[15] Sarno M, Sannino D, Leone C, Ciambelli P. CNTs tuning and vertical alignment in anodic aluminium oxide. J Nat Gas Chem 2012;21(6):647–52.
[16] Fernandez-Romero L, Montero-Moreno JM, Pellicer E, Peiro F, Pellicer E, Peiro F, et al. Assessment of the thermal stability of anodic alumina membranes at high temperatures. Mater Chem Phys 2008;111(2–3):542–7.
[17] Wernick S, Pinner R. The surface treatment and finishing of alumimum and its alloys. 4th ed. Teddington: Robert Draper Ltd.; 1972. p. 508.
[18] Zhou J, Wu J, Yang Y. Research on the thermal expansion behavior of anodic films on aluminium. Thin Solid Films 1999;346(1–2):280–3.
[19] Goueffon T, Mabru C, Labarrère M, Arurault L, Tonon C, Guigue P. Investigations into the coefficient of thermal expansion of porous films prepared on AA7175 T7351 by anodizing in sulphuric acid electrolyte. Surf Coat Tech 2010;205(7):2643–8.
[20] Schneider JJ, Maksimova NI, Engstler J, Joshi R, Schierholz R, Feile R. Catalyst free growth of a carbon nanotube-alumina composite structure. Inorg Chim Acta 2008;3615(6):1770–8.
[21] Lebedeva IV, Knizhnika AA, Gavrikova AV, Baranova AE, Potapkin BV, et al. First-principles based kinetic modeling of effect of hydrogen on growth of carbon nanotubes. Carbon 2011;49(7):2508–21.
[22] Hidaka Y, Nishimori T, Sato K, Henmi Y, Okuda R, Inami K. Shock-tube and modeling study of ethylene pyrolysis and oxidation. Comb Flam 1999;117(4):755–76.
[23] Norinaga K, Janardhanan VM, Deutschmann O. Detailed chemical kinetic modeling of pyrolysis of ethylene, acetylene, and propylene at 1073–1373 K with a plug-flow reactor model. Int J Chem Kinet 2008;40(4):199–208.
[24] Di Leo RA, Landi BJ, Raffaelle RP. Purity assessment of multiwalled carbon nanotubes by Raman spectroscopy. J Appl Phys 2007;101:064307.
[25] Di Bartolomeo A, Sarno M, Giubileo F, Altavilla C, Lemmo L, Piano S, et al. Multiwalled carbon nanotube films as small-sized temperature sensors. J Appl Phys 2009;105:064518-1–6.
[26] Kim P, Zheng Y, Agnihotri S. Adsorption equilibrium and kinetics of water vapor in carbon nanotubes and its comparison with activated carbon. Ind Eng Chem Res 2008;47(9):3170–8.
[27] Zhao J, Buldum A, Han J, Lu JP. Gas molecule adsorption in carbon nanotubes and nanotube bundles. Nanotechnology 2002;13(2):195–200.
[28] Holt JK, Park HG, Wang Y, Stadermann M, Artyukhin AB, Grigoropoulos CP, et al. Fast mass transport through sub-2-nanometer carbon nanotubes. Science 2006;312(5776):1034–7.
[29] Altalhi T, Ginic-Markovic M, Han N, Clarke S, Losic D. Synthesis of carbon nanotube (CNT) composite membranes. Membranes 2011;1(1):37–47.